Breaking Barriers in Crosslinking Mass Spectrometry: Enhanced Throughput and Sensitivity with the Orbitrap Astral Mass Analyzer

Fränze Müller[1*], Karel Stejskal[3], Karl Mechtler[1,2,3*]

[1]Research Institute of Molecular Pathology (IMP), Vienna BioCenter (VBC), Vienna, Austria.
[2]Gregor Mendel Institute of Molecular Plant Biology (GMI), Austrian Academy of Sciences, Vienna BioCenter (VBC), Vienna, Austria.
[3]Institute of Molecular Biotechnology (IMBA), Austrian Academy of Sciences, Vienna BioCenter (VBC), Vienna, Austria.

*Corresponding authors: fraenze.mueller@imp.ac.at; karl.mechtler@imp.ac.at

Keywords: crosslinking mass spectrometry, quality control, Orbitrap Astral, Orbitrap Eclipse, compensation voltage, fragmentation, HCD

Author contributions:

Fränze Müller supervised, conceptualized the study, designed the MS experiments, performed data analysis, and wrote the manuscript, **Karel Stejskal** maintained and equipped the Orbitrap Eclipse instrument, corrected the manuscript and provided advice for instrument setups, **Karl Mechtler** supervised the study. All authors revised and agreed on the manuscript.

Abstract

The advancement of crosslinking mass spectrometry (CLMS) has significantly enhanced the ability to study protein-protein interactions and complex biological systems. This study evaluates the performance of the Orbitrap Astral and Eclipse mass spectrometers in CLMS workflows, focusing on the identification of low-abundance crosslinked peptides. The comparison employed consistent liquid chromatography setups and experimental conditions, using Cas9 crosslinked with PhoX and DSSO as quality control samples. Results demonstrated that the Astral analyzer outperformed the Eclipse, achieving over 40% more unique residue pairs (URP) due to its superior sensitivity and dynamic range, attributed to its multi-reflection time-of-flight analyzer and nearly lossless ion transmission. Additionally, the study revealed that single higher-energy collisional dissociation (HCD) fragmentation methods significantly outperformed stepped HCD methods on the Astral, while the Eclipse maintained similar performance across both approaches. Gradient optimization experiments further highlighted the impact of separation times on crosslink identifications, with longer gradients yielding higher identification rates. Collectively, this work underscores the importance of instrumentation choice, fragmentation strategies, and method optimization in maximizing CLMS performance for protein interaction studies.

Introduction

Crosslinking mass spectrometry (CLMS) has become a vital tool for studying protein-protein interactions and the three-dimensional architecture of biological systems. By chemically linking interacting residues and analyzing these crosslinked peptides, CLMS complements traditional techniques like cryo-electron microscopy and X-ray crystallography, providing unique insights into protein structures and interactions[1–8]. These complementary insights are

invaluable for understanding the intricate interactions underlying cellular machinery and for constructing more comprehensive models of protein complexes[9–12]. Recent advances in CLMS have focused on enhancing crosslinking chemistry, instrumentation, and data analysis. New crosslinkers, including photoactivatable and isotopically labelled reagents, improve specificity and sensitivity, enabling studies of dynamic interactions in native environments[13,14]. CLMS extends to in vivo systems, revealing transient interactions in detail[15–17]. Integrative approaches combining CLMS with computational tools like AlphaFold and AlphaLink with cryo-EM enable comprehensive mapping of interaction networks and conformational dynamics[18–20].

Despite its promise, the success of CLMS heavily relies on the performance of the mass spectrometric instrumentation, which must be capable of managing complex peptide mixtures while delivering high-resolution and accurate mass measurements. Recent advancements in Orbitrap mass spectrometers, particularly the Thermo Scientific Orbitrap Astral[21,22] and Eclipse[23,24] instruments, have introduced new capabilities that can significantly enhance crosslinking data acquisition and interpretation. These instruments leverage Orbitrap technology, renowned for its high resolving power, mass accuracy, and dynamic range, all of which are crucial for CLMS, where crosslinked peptides are often present in low abundance and require precise identification.

The Astral and Eclipse Orbitrap instruments present distinct advantages over previous generations of mass spectrometers in terms of sensitivity, speed, and operational features, which impact their respective performance in CLMS workflows. The Orbitrap Eclipse is equipped with an advanced ion-routing multipole and a versatile scan strategy that allows for rapid switching between different fragmentation techniques, such as higher-energy collisional dissociation (HCD) and collision-induced dissociation (CID). Furthermore, it offers an advanced ion management technology (AIM+) and a QR5 segmented quadrupole mass filter, which enhances mass selection precision, contributing to improved detection of low-abundance peptides and it features an advanced peak determination (APD) algorithm, which improves precursor annotation in data-dependent experiments, further enhancing the detection of low-abundance crosslinked peptides. This flexibility supports broader sequence coverage, providing better identification of peptides[25] and therefore potentially also of crosslinked species. On the other hand, the Astral instrument utilizes a novel multi-reflection time-of-flight (MR ToF) analyzer with isochronous drift in elongated ion mirrors[21,22]. This innovative design significantly improves resolving power while maintaining high sensitivity, which is especially important for low-abundance peptide species like crosslinks. Furthermore, the Astral employs an "Asymmetric Track Lossless" mode for ion transmission, resulting in nearly lossless ion movement and enhanced sensitivity for data acquisition, making it potentially highly effective for CLMS applications[21,22]. Compared to the Eclipse, the Astral shows notable improvements in sensitivity and throughput, quantifying significantly more peptides per unit time and offering high-quality quantitative measurements across a wide dynamic range[25]. These features would allow for deeper exploration of protein interaction networks, especially in workflows involving challenging, low-abundance crosslinked peptides.

This study compares the performance of the Orbitrap Eclipse and Astral mass spectrometers in the context of crosslinking mass spectrometry workflows. By highlighting the respective strengths of each instrument, we aim to provide researchers with a clearer understanding of the optimal choice for their specific CLMS applications.

Results

To compare the performance of both instruments, we used the very same liquid chromatography (LC) setup equipped with a 25 cm IonOpticks Aurora Ultimate column. Cas9-Helo protein was crosslinked with either PhoX (DSPP) or DSSO and used as a quality control (QC) sample throughout the entire experimental series. To ensure that the difference in results is unique to the instruments, the QC samples were produced in a bigger batch of 100 µg total protein amount for each crosslinker and frozen in aliquots for long-term storage. Aliquots from the same batch were always injected on both instruments equally to reduce variability coming from the crosslink reaction and sample preparation procedure. Both instruments were equipped with high-field asymmetric-waveform ion-mobility spectrometry (FAIMS) devices for ion filtering and noise reduction during data acquisition. LC setup, gradient design, and acquisition methods were kept as similar as possible for both instruments (Figure 1). Compensation voltages (CV) were optimised for the Orbitrap Astral as shown in supplemental Figures S2, S3 and S4. According to previous publications, CV values for the Eclipse measurements were selected as CV -50 V, -60 V, and -70 V[26].

Figure 1: Overview of the experiment design. QC samples Cas9 crosslinked with PhoX or DSSO were injected on Astral or Eclipse instruments in parallel with single or stepped higher-energy collisional dissociation (HCD) methods to compare the performance of the instruments and fragmentation methods. Proteome Discoverer and MS Annika were used for database search and data validation.

Optimisation of CV values for Astral measurements

Each CV value was acquired separately to find the best-performing value, followed by a combinatorial approach using the Upset plot function in Python to evaluate the best combination of 3 CV values for enhanced crosslink identification. CVs were acquired from -30 to -90 V, with -48 V showing the best results for single injections (Figure S2) reaching 326 unique residue pairs. All possible combinations of CV values have been analysed using the Upset plot function, resulting in three combinations of interest. CV -48 V, -60 V, -75 V were selected to achieve the highest number of crosslinks with the least overlap, CV -48, -55, -90 V were selected to have the least overall overlap and CV -40 V, -48 V, -60 V to have the highest overlap (Figure S3B). These combinations were tested with an injection amount of 100 ng and compared with our control CV combination of -48 V, -60 V, -80 V for QC runs. The combination with the highest number of crosslinks but the least overlap (-48 V, -60 V, -75 V) surpassed other combinations with 569 unique residue pairs, 20.6% more than the CV combination with -40 V, -48 V, -60 V (40 V, -50 V, -60 V, Figure S4). Please note, that optimal CV values may vary between FAIMS devices and should therefore be individually evaluated for each instrument.

Instrument comparison

The comparison of the Astral and Eclipse instruments for the identification of crosslinks using both non-cleavable (PhoX) and cleavable (DSSO) crosslinkers are illustrated by injecting dilution series from 1 ng to 500 ng of crosslinked Cas9 protein for both crosslinkers on both instruments in parallel. The maximum number of unique crosslinks was achieved at 250 ng for PhoX and 500 ng for DSSO (Figure 2). In both cases, the Astral mass analyzer significantly outperformed the Eclipse by over 40%. Interestingly, 192 and 121 unique residue pairs could be identified with 1 ng injection amount for PhoX and DSSO, respectively. This improvement is attributed to the enhanced sensitivity of Astral's multi-reflection time-of-flight (MR ToF) analyzer, which is particularly effective in maintaining resolution for low-abundance species.

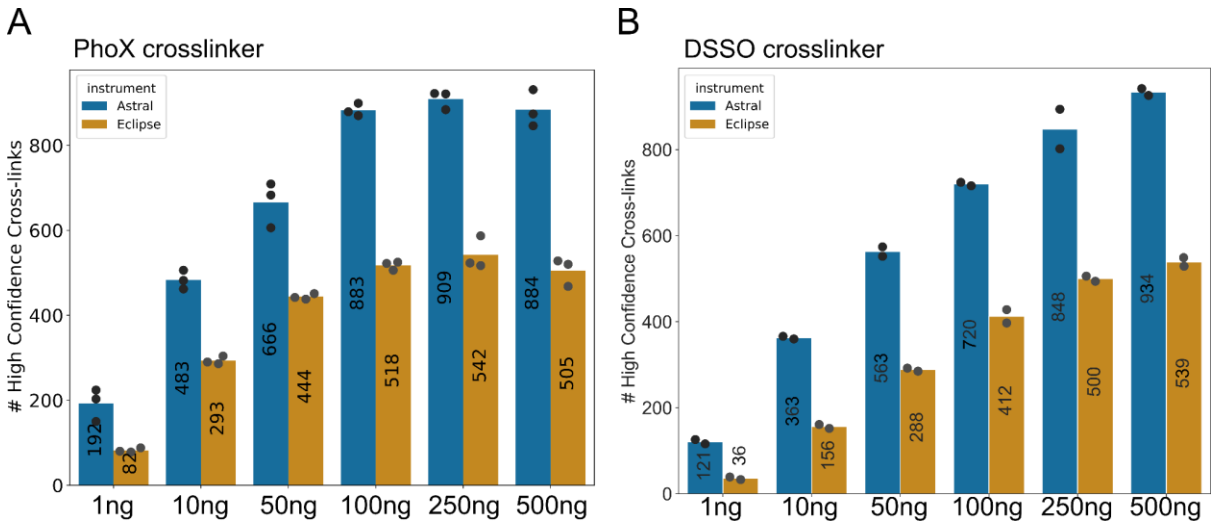

Figure 2: Comparison of Astral and Eclipse crosslinking data for PhoX (non-cleavable) and DSSO (cleavable) crosslinker. A: Dilution series of Cas9 crosslinked with PhoX starting from 1ng to 500 ng acquired on Eclipse and Astral in triplicates. The maximum number of unique crosslinks is reached with 250 ng and plateaus afterwards. The Astral mass analyser (blue) outperforms the Eclipse (orange) data by more than 40%. B: Dilution series of Cas9 crosslinked with DSSO starting from 1ng to 500 ng acquired on Eclipse and Astral in duplicates. The maximum number of unique crosslinks is reached with 500 ng. The Astral mass analyser (blue) outperforms the Eclipse (orange) data again by more than 40% for DSSO.

The observed difference of 40% in crosslinking identification between the two instruments cannot be attributed entirely to speed, as the average crosslink spectrum match (CSM) count per unique residue pair (URP) was 5.9 for Astral versus 6.2 for Eclipse on PhoX samples, and 3.5 for both instruments on DSSO samples. Score distributions between both instruments were also similar (data not shown), indicating that better spectral quality alone cannot explain the improved identification rates for the Astral mass spectrometer. The main advantage of the Astral for crosslinking samples may stem from the simultaneous utilization of Orbitrap for MS1 and the Astral analyzer for MS2 analysis. This setup ensures that MS2 spectra are recorded with high resolution and reduced noise, enhancing the sensitivity and dynamic range that benefits crosslinking data.

<u>Fragmentation strategy comparison on Astral and Eclipse</u>

Previous publications suggest a benefit for stepped higher-energy collisional dissociation (HCD) fragmentation over single HCD for cleavable crosslinkers. To test this hypothesis also for the Orbitrap Astral mass analyser, Cas9 crosslinked with PhoX or DSSO was injected again as a dilution series ranging from 1 ng to 500 ng injection amount with a stepped HCD and single HCD method. For both crosslinkers, PhoX and DSSO, single HCD consistently outperformed stepped HCD in terms of the number of unique crosslinks identified (Figure 3). Maximum performance could be achieved with 250 ng injection amount for PhoX samples with 909 URP single HCD and 726 URP stepped HCD resulting in 25% increase using just a single HCD for fragmentation. Interestingly, the benefit for single HCD methods stays constant across all injection amounts with improved identification rates between 19% and 26% (Figure 3A). Similar observations could be made for the cleavable crosslinker DSSO. Using 250 ng injection amounts the DSSO sample could gain 20% more identifications with a single HCD method instead of a stepped HCD method (single: 848 URP, stepped: 707 URP). The benefit

of the single HCD method was more profound with low injection amounts (1 ng 39%) than for higher injection amounts (500 ng 18%) for the DSSO experiments (Figure 3C). The effect for single HCD methods could be only observed on the Astral mass spectrometer. Comparing the difference between single HCD and stepped HCD on the Eclipse, the stepped HCD method with PhoX samples and 100 ng injection amount outperformed the single HCD method not-significantly by 1.5%. This is also true for DSSO samples with 7.4% gain for stepped HCD (Figure 3B, PhoX and D, DSSO).

The Astral mass spectrometer appears to benefit significantly from single HCD fragmentation due to its optimized ion transmission efficiency. The system is likely better suited to a straightforward, focused ion path, contrary to the complexity introduced by stepped fragmentation. Stepped HCD offers little advantage on the Astral as the extended scan times required conflict with the instrument's design for rapid data acquisition. By using single HCD, the Astral's highly sensitive and high-resolution detection capabilities can be fully leveraged without additional complications that may arise from stepped HCD methods. In contrast, the Orbitrap Eclipse is equipped with advanced ion management technologies such as AIM+ and a segmented quadrupole mass filter. These features provide precise control over ion selection and handling, allowing the Eclipse to adapt effectively to different fragmentation methods. This adaptability may help the Eclipse handle stepped HCD efficiently, thereby minimizing any potential drawbacks of the additional complexity. The advanced control mechanisms ensure effective ion transmission in both single and stepped HCD modes, which explains why the observed differences in crosslinking performance are less pronounced compared to the Astral. These findings highlight the importance of careful optimization of fragmentation methods to maximize the performance of high-resolution mass spectrometers, with specific considerations for each instrument's strengths.

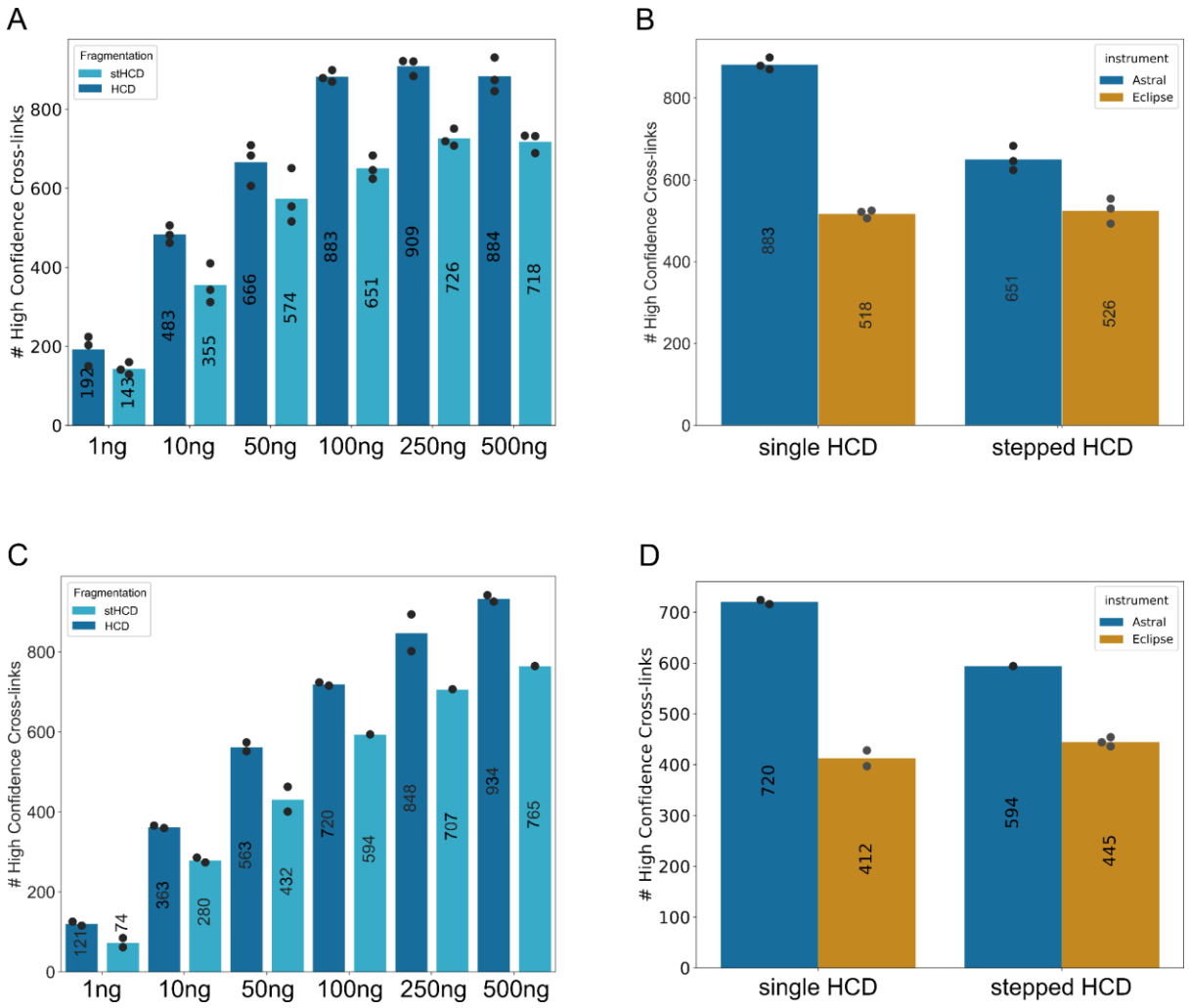

Figure 3: Comparison of single and stepped HCD for PhoX (non-cleavable) and DSSO (cleavable) crosslinker. A: Comparison between single HCD (dark blue) and stepped HCD (light blue) of the PhoX dilution series on the Orbitrap Astral. Single HCD shows higher numbers of unique crosslinks as stepped HCD for all injections amounts. B: Direct view on the difference between stepped and single HCD acquired on both instruments for 100 ng. The difference between single HCD and stepped HCD is dominant for Astral data (blue) but not significantly different for Eclipse data (orange). C: Comparison between single HCD (dark blue) and stepped HCD (light blue) of the DSSO dilution series on the Orbitrap Astral. Single HCD shows also increased numbers of unique crosslinks as stepped HCD for the DSSO dilution series. D: Direct view on the difference between stepped and single HCD acquired on both instruments for 100 ng injection amounts. The difference between single HCD and stepped HCD is dominant for Astral data (blue) but not significantly different for Eclipse data (orange), same as for the PhoX samples.

Gradient optimisation for enhanced crosslink identification

In shotgun proteomics experiments, protein identifications for injection amounts up to 1 µg benefit from longer separation times, hence longer gradients[27–29]. To test this observation also for crosslinking samples, Cas9-Helo crosslinked with PhoX was injected in 100 ng amounts using active gradient times from 10 minutes to 180 minutes. The results showed a dramatic increase in the number of unique residue pairs of 868.9% (45 URP for 10min, 436 URP for 180 min) as the gradient time was extended, with a shallower slope occurring around 95 to 180 minutes (375 URP 95 min, 436 URP 180 min, Figure 4A). Notably, crosslink spectrum

match (CSM) numbers also increased with gradient length by 4495.5% (110 CSMs for 10min, 5055 CSMs for 180 min), indicating improved peptide detection and identification rates (Figure 4B). This strong increase in crosslink identifications can be explained by the increasing support of CSMs per unique residue pair for longer gradients. Using a 10 min gradient results in 2.5 CSMs per crosslink, while a 180 min gradient delivers up to 12 CSMs per crosslink (Figure 4D). Notably, the CSM/ crosslink rate does not plateau after 180 min, hence crosslink numbers could be potentially pushed further with even longer gradients but at the cost of measurement time and ultimately financial cost. However, the number of unique crosslinks per minute peaked early (between 10 to 20 minutes) and then decreased, which suggests decreasing returns in identification efficiency with extended gradients (Figure 4C). This finding supports the need for optimizing gradient length based on the experimental goals, balancing total identification with efficiency and instrument measurement time. Although maximum numbers can be achieved with very long gradients, shortening the instrument time while maintaining reasonable high identification rates could be beneficial for high throughput studies or minimising measurement costs.

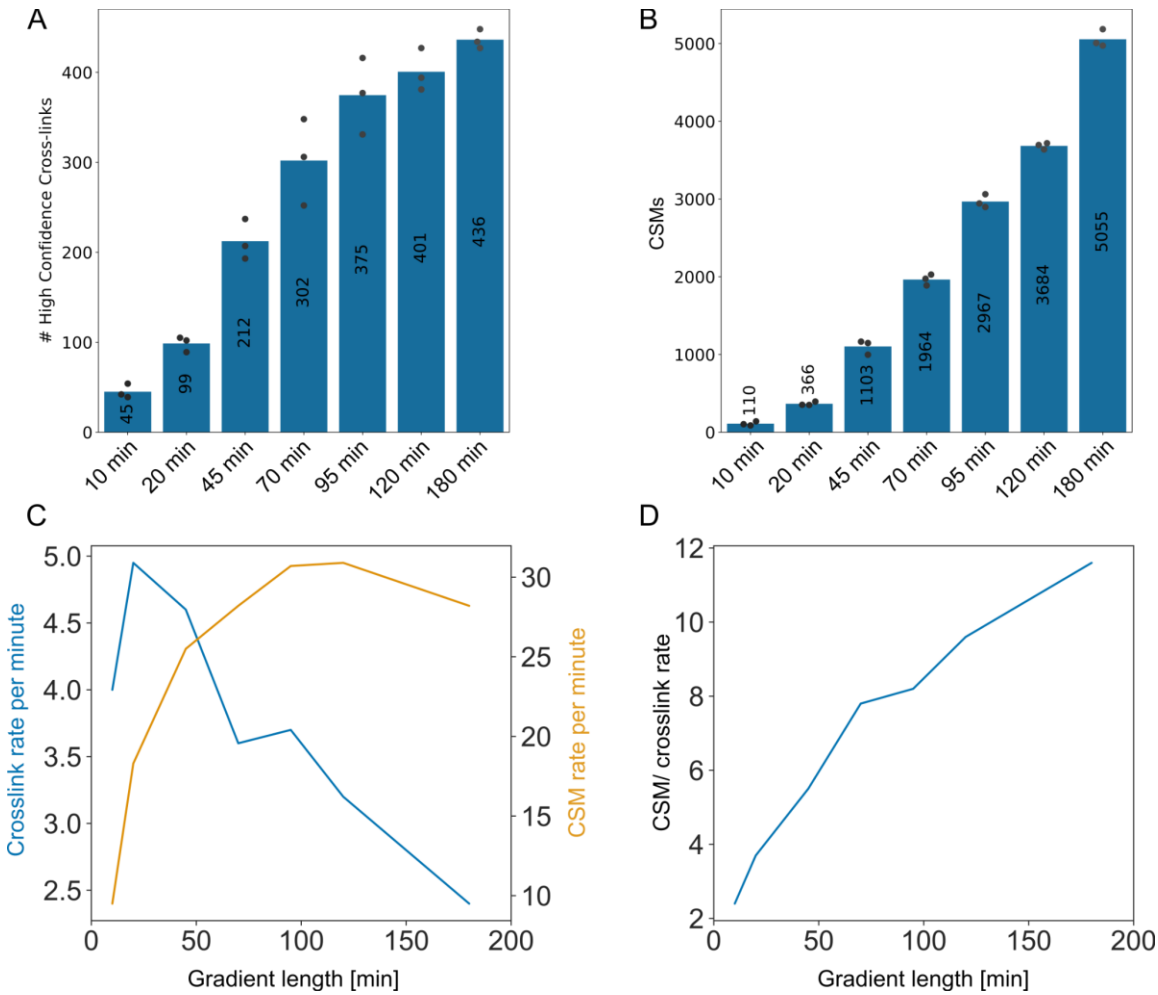

Figure 4: Gradient optimization for 250 ng Cas9 crosslinked with PhoX starting with 10 min up to 180 min on the Astral. A: Unique crosslink numbers increase dramatically with longer gradient times. Triplicate injections revealed an 868.9% increase in crosslinks from 10-minute gradients to 180-minute active gradients. The slope of increase flattens from 95 min to 180 min with a 16% raise. B: Crosslink

spectrum match numbers (CSMs) for 10 min up to 180 min gradients. The numbers of CSMs increase constantly with longer gradients by 4495.5%. C: Line plot of unique crosslinks per min in dependence of the gradient length (blue) and CSMs (orange), respectively. The number of unique crosslinks increases from 10 to 20 min but decreases dramatically thereafter from 5 to 2.5 links per minute. This is in agreement with the slower increase in crosslink numbers with longer gradients. CSMs per minute increase steeply until 120 min and keep a high level thereafter. D: Number of CSMs per unique crosslink identified. The number of CSMs per crosslink increases almost linearly with the gradient length. 10 min gradient results in 2.5 CSMs per crosslinks and increases towards 12 CSMs per link with 180 min.

Column comparison

We briefly tested a 50 cm PepMap column (Thermo Fisher Scientific) and a 25 cm Aurora Ultimate (IonOpticks) analytical reverse-phase column to evaluate the optimal separation performance for crosslinked peptides. Both columns use C18 as a stationary phase and are suitable for nano-flow setups but differ substantially in particle size, pore size, length, and pressure limit. The key parameters of both columns are summarised in supplementary Table S1. The PepMap and Aurora columns exhibit distinct characteristics that make them suitable for different analytical applications. The PepMap column, with its longer length of 50 cm and a particle size of 2 µm, is ideal for achieving high-resolution separations in complex samples, particularly when comprehensive profiling is required. Its pore size of 100 Å makes it well-suited for smaller analytes, although its pressure limit of 1500 bar may necessitate careful monitoring during high-flow operations. Conversely, the Aurora column, with its shorter length of 25 cm and smaller particle size of 1.7 µm, delivers rapid and efficient separations, making it advantageous for high-throughput analyses. Its larger pore size of 120 Å supports the analysis of larger biomolecules such as crosslinked peptides. Furthermore, the Aurora column's higher pressure tolerance (>1700 bar) offers greater robustness for demanding workflows. These potential advantages for crosslinked peptides resulted in 779 unique residue pairs (URP) for 100 ng injection of crosslinked Cas9 with PhoX, compared to 560 unique residue pairs acquired using the PepMap column. The Aurora column therefore outperformed PepMap by 28% (Figure S5). Quantitation in Skyline of 5 selected crosslinked peptides across a 70 min gradient revealed smaller full-width half maximum values for the aurora column, resulting in sharper peaks and therefore higher intensities of the selected peptides (Figure S6 A and B). Higher intensities seem to be the key point in performance difference between both columns and lead to an overall better performance of the aurora column. Furthermore, better peptide separation could be observed for the aurora column as seen in Figure S7. The chromatographic resolution of the aurora column outperformed the PepMap column despite the longer separation path of 50 cm vs. 25 cm. Effective separation requires peptides to enter the pores of the column's porous particles. When their hydrodynamic diameter is too large, access to the internal volume is reduced, causing diminished retention, peak broadening, or tailing[28]. To utilize at least 50% of the pore volume, the pore size should be three to five times larger than the peptides/ proteins hydrodynamic diameter[30,31]. 90% of theoretical human tryptic peptides have a molecular weight of less than 3 kDa (with two missed cleavages, only 10% exceed 5.6 kDa) and hydrodynamic diameters below 100 Å[28]. Crosslinked peptides typically have larger molecular weights because they are formed by the combination of two peptides along with the added mass of the crosslinker[32]. As a result, they require larger pore sizes for effective separation compared to linear peptides. The larger pore size of the Aurora column (120 Å vs 100 Å PepMap) likely enhanced here the binding of larger crosslinked peptides. Despite the pore size, the Aurora column most likely also benefits from the smaller particle size of 1.7 µm instead of 2 µm, because column efficiency is usually proportional to the particle

diameter[28,33], hence smaller particle size improves the separation of peptides. Furthermore, the IonOpticks column features enhanced ionisation efficiency due to its smaller emitter diameter (approximately 6 µm) compared to the PepMap emitter setup using a fused silica emitter (10 µm) with integrated liquid junction (MSWIL, Supplier: Bruker).

Conclusion

Overall, the Orbitrap Astral mass analyser demonstrated superior performance across all tested conditions, particularly in terms of sensitivity and the number of crosslinks identified. The increased throughput and enhanced analytical capabilities of the Orbitrap Astral make it an ideal choice for CLMS workflows, especially when dealing with low-abundant crosslinked peptides or when seeking to achieve deeper proteome coverage. The Orbitrap Eclipse, while still capable, showed limitations in sensitivity and efficiency when compared directly with the Orbitrap Astral. These results suggest that the Astral mass spectrometer is highly advantageous for studies requiring high sensitivity, efficient crosslinking identification, and comprehensive protein interaction mapping.

The data presented in this study emphasize the impact of advanced instrumentation, fragmentation techniques, and optimized gradients on CLMS performance. Researchers can utilize these insights to better choose appropriate instrumentation and optimize workflows for their specific biological questions, ultimately contributing to a more detailed understanding of protein interactions and structural biology.

We are very excited about current developments in the crosslinking field in the direction of predicted crosslink fragment intensities and new rescoring functions within the Prosit-XL software[34] package and we hope to apply this pipeline soon to our Astral crosslinking data to further boost the crosslink identification.

Methods

Reagents

Table S1. Special reagents used for comparing the Orbitrap Astral and Orbitrap Eclipse mass spectrometers.

Reagent name	Catalogue number	Supplier
Cas9 from *S. pyogenes* fused with a Halo-tag	In house	Deng *et al*.[35]
Trypsin gold	V5280	Promega
PhoX (DSPP)	A52286	Thermo Fisher Scientific
DSSO	A33545	Thermo Fisher Scientific

Aurora Ultimate	AUR3-25075C18	IonOpticks
PepMap	DNV75500PN	Thermo Fisher Scientific
Fused silica emitter (ID 10 um, OD 150 um)	PSFSE 10 (1893527)	MSWIL (Supplier: Bruker)

Crosslinking reaction for Cas9

Cas9-Halo protein was crosslinked using either PhoX or DSSO. All crosslinkers were prepared as stock solutions at a concentration of 50 mM in dry Dimethyl Sulfoxide (DMSO). For the crosslinking reaction, Cas9 was diluted in 50 mM HEPES to achieve a final protein concentration of 1 µg/uL and a crosslinker was added to a final concentration of 1 mM (PhoX) or 0.2 mM (DSSO). After a 45-minute incubation on ice, the reactions were stopped using 100 mM Tris buffer. Each crosslink reaction was prepared in parallel with the same conditions and buffers.

In-Solution Digest

For the in-solution digest, proteins were reduced using 10 mM Dithiothreitol (DTT) for 30 minutes at 50°C, followed by water bath sonication for 10 min and finally alkylated using 50 mM Iodoacetamide (IAA) for 30 min in the dark. The digest was performed using Trypsin (1:100, enzyme-to-protein ratio). The mixture was incubated overnight at 37°C to facilitate complete digestion. The digestion process was terminated by the addition of 10% Trifluoroacetic Acid (TFA), adjusting to a final concentration of 0.2%.

Mass spectrometry

LC-MS/MS analysis was performed using an Orbitrap Eclipse or Orbitrap Astral mass spectrometer with high-field asymmetric ion mobility spectrometry (FAIMS) interface (FAIMS Pro Duo, Thermo Fisher Scientific, Waltham, Massachusetts, United States) coupled with an EASY-Spray source and Vanquish Neo UHPLC system (Thermo Fisher Scientific). A trap column PepMap C18 (5 mm × 300 µm ID, 5 µm particles, 100 Å pore size) (Thermo Fisher Scientific, Waltham, Massachusetts, United States) and an analytical column PepMap C18 (500 mm × 75 µm ID, 2 µm, 100 Å) (Thermo Fisher Scientific, Waltham, Massachusetts, United States) or Aurora Ultimate (250 mm × 75 µm ID, 1.7 µm, 120 Å)(IonOpticks, Fitzroy, Australia) were employed for separation. The column temperature was set to 50°C. Sample loading was performed using 0.1% trifluoroacetic acid in water with a flow rate of 25 uL/min. Mobile phases used for separation were as follows: A 0.1% formic acid (FA) in water; B 80% acetonitrile, 0.1% FA in water. Peptides were eluted using a flow rate of 230 nL/min (PepMap) or 300 nL/min (Aurora), with the following gradient: from 2% to 37% phase B in 60 min, from 37% to 47% phase B in 10 min, from 47% to 95% phase B in 1 min, followed by a washing step at 95% for 4 min, and re-equilibration of the column. The gradient was altered for the gradient optimization experiments to facilitate longer gradients.

The mass spectrometry settings on the Astral mass spectrometer were set as follows: FAIMS separation was performed with the following settings: inner and outer electrode temperatures

were 100°C, FAIMS carrier gas flow was 3.5 L/min, compensation voltages (CVs) of −48, −60, and −75 V were used in a stepwise mode during the analysis. The FAIMS CV values were measured in a range from -30 to -90 in single measurements during the CV optimisation experiment. -48 V has been selected instead of -50 V according to the paper of Bubis *et al.* 2025[36]. The ion transfer tube temperature was set to 275°C. The mass spectrometer was operated in a data-dependent mode with cycle time 1s, using the following full scan parameters: *m/z* range 375-1300, nominal resolution of 180 000, with a target of 500% charges for the automated gain control (AGC), and a maximum injection time of 6 ms. For higher-energy collisional dissociation (HCD) MS/MS scans, single normalised collision energy (NCE) of 32% (PhoX) and 30% (DSSO) was used for single HCD experiments and stepped HCD values of 25%; 27%; 32% for PhoX[37] and 21%; 25%; 32% for DSSO[38,39]. Precursor ions were isolated in a 1.6 Th (+/- 0.8 Th) window with no offset and accumulated for a maximum of 20 ms or until the AGC target of 500% was reached. Precursors of charge states from 3+ to 6+ were scheduled for fragmentation. Previously targeted precursors were dynamically excluded from fragmentation for 15 seconds. The sample load was typically in a range of 1 ng to 500 ng as indicated in the respective figure or with 100 ng for the column comparison and 250 ng for the gradient optimization experiments. Detailed parameters can be found in each raw file under the instrument method section.

The mass spectrometry settings on the Eclipse mass spectrometer were set as follows: FAIMS separation was performed with the following settings: inner and outer electrode temperatures were 100°C, FAIMS carrier gas flow was 4.4 L/min, compensation voltages (CVs) of −50, −60, and −70 V were used in a stepwise mode during the analysis. The ion transfer tube temperature was set to 275°C. The mass spectrometer was operated in a data-dependent mode with cycle time 1s, using the following full scan parameters: *m/z* range 375-1300, nominal resolution of 120 000, with a target of 100% charges for the automated gain control (AGC), and a maximum injection time of 100 ms. For higher-energy collisional dissociation (HCD) MS/MS scans, single normalised collision energy (NCE) of 32% (PhoX) and 30% (DSSO) was used for single HCD experiments and stepped HCD values of 25%; 27%; 32% for PhoX and 21%; 25%; 32% for DSSO. Precursor ions were isolated in a 1.6 Th window with no offset and accumulated for a maximum of 70 ms or until the AGC target of 500% was reached. The resolution for MS2 scans was set to 30000. Precursors of charge states from 3+ to 6+ were scheduled for fragmentation. Previously targeted precursors were dynamically excluded from fragmentation for 15 seconds.

Data analysis

Raw files were analysed using Thermo Proteome Discoverer (v. 3.1.0.638). Searches were performed against the Cas9 sequence (Uniprot ID: Q99ZW2) plus a Crapome database (downloaded from https://www.thegpm.org/crap/).

Linear peptides were identified using MS Amanda search engine (v. 3.0.20.558)[40] and the crosslinked peptides were identified using MS Annika (v. 3.0)[41–43]. The search workflow included a recalibration step for each file, followed by a first search using MS Amanda to identify linear peptides and monolinks. Subsequently, spectra with highly confident identifications of a linear peptide were filtered out and not considered for the cross-link search. Finally, a crosslink search was performed using MS Annika. The workflow used in Proteome Discoverer is shown in Figure S8. Search parameters for linear and crosslink searches can

be found in Supplementary Table 2. The FDR was estimated using the MS Annika validator node with 1% FDR (high confidence) for Cas9 crosslinking data on CSM and residue pair levels. The FDR calculation is based on a target-decoy approach[41].

For data filtering and visualisation Python 3.9.7 was used with the following packages: pandas (v 1.3.4)[44], numpy (v 1.20.3)[44,45], matplotlib (v 3.4.3)[46] (pyplot, venn (v 0.11.6)), seaborn (v 0.11.2)[47], scipy (v 1.7.1) and bioinfokit (v 1.0.8)[48,49].

Data availability

The mass spectrometry proteomics data have been deposited to the ProteomeXchange Consortium (http://proteomecentral.proteomexchange.org) via the PRIDE partner repository[50,51] with the dataset identifier PXD059096.

References

1. Sinz, A. Divide and conquer: cleavable cross-linkers to study protein conformation and protein-protein interactions. *Anal. Bioanal. Chem.* **409**, 33–44 (2017).
2. Petrotchenko, E. V. & Borchers, C. H. Crosslinking combined with mass spectrometry for structural proteomics. *Mass Spectrom. Rev.* **29**, 862–876 (2010).
3. Sinz, A. Cross-Linking/Mass Spectrometry for Studying Protein Structures and Protein-Protein Interactions: Where Are We Now and Where Should We Go from Here? *Angew. Chem. Int. Ed Engl.* **57**, 6390–6396 (2018).
4. Yu, C. & Huang, L. Cross-linking mass spectrometry: An emerging technology for interactomics and structural biology. *Anal. Chem.* **90**, 144–165 (2018).
5. O'Reilly, F. J. *et al.* Protein complexes in cells by AI-assisted structural proteomics. *Mol. Syst. Biol.* **19**, e11544 (2023).
6. Wheat, A. *et al.* Protein interaction landscapes revealed by advanced in vivo cross-linking-mass spectrometry. *Proc. Natl. Acad. Sci. U. S. A.* **118**, e2023360118 (2021).
7. Petrotchenko, E. V. & Borchers, C. H. Protein Chemistry Combined with Mass Spectrometry for Protein Structure Determination. *Chem Rev* **122**, 7488–7499 (2022).
8. Graziadei, A. & Rappsilber, J. Leveraging crosslinking mass spectrometry in structural and cell biology. *Structure* **30**, 37–54 (2022).

9. Yugandhar, K. *et al.* MaXLinker: Proteome-wide Cross-link Identifications with High Specificity and Sensitivity. *Mol. Cell. Proteomics* **19**, 554–568 (2020).
10. Liu, F., Rijkers, D. T. S., Post, H. & Heck, A. J. R. Proteome-wide profiling of protein assemblies by cross-linking mass spectrometry. *Nat. Methods* **12**, 1179–1184 (2015).
11. Liu, F., Lössl, P., Scheltema, R., Viner, R. & Heck, A. J. R. Optimized fragmentation schemes and data analysis strategies for proteome-wide cross-link identification. *Nat. Commun.* **8**, 15473 (2017).
12. Götze, M., Iacobucci, C., Ihling, C. H. & Sinz, A. A Simple Cross-Linking/Mass Spectrometry Workflow for Studying System-wide Protein Interactions. *Anal. Chem.* **91**, 10236–10244 (2019).
13. Nie, M. & Li, H. Innovation in Cross-Linking Mass Spectrometry Workflows: Toward a Comprehensive, Flexible, and Customizable Data Analysis Platform. *J Am Soc Mass Spectrom* **34**, 1949–1956 (2023).
14. Yugandhar, K., Zhao, Q., Gupta, S., Xiong, D. & Yu, H. Progress in methodologies and quality-control strategies in protein cross-linking mass spectrometry. *Proteomics* **21**, e2100145 (2021).
15. Lu, H., Zhu, Z., Fields, L., Zhang, H. & Li, L. Mass Spectrometry Structural Proteomics Enabled by Limited Proteolysis and Cross-Linking. *Mass Spectrom Rev* (2024) doi:10.1002/mas.21908.
16. Debelyy, M. O., Waridel, P., Quadroni, M., Schneiter, R. & Conzelmann, A. Chemical crosslinking and mass spectrometry to elucidate the topology of integral membrane proteins. *PLoS One* **12**, e0186840 (2017).
17. Weerasekera, R. & Schmitt-Ulms, G. Crosslinking strategies for the study of membrane protein complexes and protein interaction interfaces. *Biotechnol Genet Eng Rev* **23**, 41–62 (2006).
18. Yu, C. & Huang, L. New advances in cross-linking mass spectrometry toward structural systems biology. *Curr Opin Chem Biol* **76**, 102357 (2023).
19. Stahl, K., Graziadei, A., Dau, T., Brock, O. & Rappsilber, J. Protein structure prediction

with in-cell photo-crosslinking mass spectrometry and deep learning. *Nat. Biotechnol.* **41**, 1810–1819 (2023).

20. Stahl, K. *et al.* Modelling protein complexes with crosslinking mass spectrometry and deep learning. *Nat Commun* **15**, 7866 (2024).
21. Stewart, H. *et al.* A Conjoined Rectilinear Collision Cell and Pulsed Extraction Ion Trap with Auxiliary DC Electrodes. *J Am Soc Mass Spectrom* **35**, 74–81 (2024).
22. Multi-reflection Astral mass spectrometer with isochronous drift in elongated ion mirrors. *Nuclear Instruments and Methods in Physics Research Section A: Accelerators, Spectrometers, Detectors and Associated Equipment* **1060**, 169017 (2024).
23. Yu, Q. *et al.* Benchmarking the Orbitrap Tribrid Eclipse for Next Generation Multiplexed Proteomics. *Anal Chem* **92**, 6478–6485 (2020).
24. Senko, M. W. *et al.* Novel Parallelized Quadrupole/Linear Ion Trap/Orbitrap Tribrid Mass Spectrometer Improving Proteome Coverage and Peptide Identification Rates. (2013) doi:10.1021/ac403115c.
25. Heil, L. R. *et al.* Evaluating the Performance of the Astral Mass Analyzer for Quantitative Proteomics Using Data-Independent Acquisition. *J Proteome Res* **22**, 3290–3300 (2023).
26. Schnirch, L. *et al.* Expanding the Depth and Sensitivity of Cross-Link Identification by Differential Ion Mobility Using High-Field Asymmetric Waveform Ion Mobility Spectrometry. *Anal Chem* **92**, 10495–10503 (2020).
27. Stejskal, K. *et al.* Deep Proteome Profiling with Reduced Carryover Using Superficially Porous Microfabricated nanoLC Columns. *Anal Chem* **94**, 15930–15938 (2022).
28. Lenčo, J. *et al.* Reversed-Phase Liquid Chromatography of Peptides for Bottom-Up Proteomics: A Tutorial. *Journal of Proteome Research* (2022) doi:10.1021/acs.jproteome.2c00407.
29. Matzinger, M. *et al.* Micropillar arrays, wide window acquisition and AI-based data analysis improve comprehensiveness in multiple proteomic applications. *Nat Commun* **15**, 1019 (2024).

30. Gritti, F. & Guiochon, G. Comparison between the loading capacities of columns packed with partially and totally porous fine particles. What is the effective surface area available for adsorption? *J Chromatogr A* **1176**, 107–122 (2007).
31. Gritti, F., Horvath, K. & Guiochon, G. How changing the particle structure can speed up protein mass transfer kinetics in liquid chromatography. *J Chromatogr A* **1263**, 84–98 (2012).
32. Expanding the Chemical Cross-Linking Toolbox by the Use of Multiple Proteases and Enrichment by Size Exclusion Chromatography. *Molecular & Cellular Proteomics* **11**, M111.014126 (2012).
33. Using long columns to quantify over 9200 unique protein groups from brain tissue in a single injection on an Orbitrap Exploris 480 mass spectrometer. *Journal of Proteomics* **308**, 105285 (2024).
34. Kalhor, M. *et al.* Prosit-XL: enhanced cross-linked peptide identification by accurate fragment intensity prediction to study protein-protein interactions and protein structures. *bioRxiv* 2024.12.15.627797 (2024) doi:10.1101/2024.12.15.627797.
35. Deng, W., Shi, X., Tjian, R., Lionnet, T. & Singer, R. H. CASFISH: CRISPR/Cas9-mediated in situ labeling of genomic loci in fixed cells. *Proc. Natl. Acad. Sci. U. S. A.* **112**, 11870–11875 (2015).
36. Bubis, J. A. *et al.* Challenging the Astral mass analyzer to quantify up to 5,300 proteins per single cell at unseen accuracy to uncover cellular heterogeneity. *Nat Methods* (2025) doi:10.1038/s41592-024-02559-1.
37. Steigenberger, B., Pieters, R. J., Heck, A. J. R. & Scheltema, R. A. PhoX: An IMAC-Enrichable Cross-Linking Reagent. *ACS Cent Sci* **5**, 1514–1522 (2019).
38. Stieger, C. E., Doppler, P. & Mechtler, K. Optimized Fragmentation Improves the Identification of Peptides Cross-Linked by MS-Cleavable Reagents. *J Proteome Res* **18**, 1363–1370 (2019).
39. Rappsilber, J. Finding and using diagnostic ions in collision induced crosslinked peptide fragmentation spectra. *International Journal of Mass Spectrometry* **444**, 116184 (2019).

40. Dorfer, V. *et al.* MS Amanda, a Universal Identification Algorithm Optimized for High Accuracy Tandem Mass Spectra. (2014) doi:10.1021/pr500202e.
41. Pirklbauer, G. J. *et al.* MS Annika: A New Cross-Linking Search Engine. *J. Proteome Res.* (2021) doi:10.1021/acs.jproteome.0c01000.
42. Birklbauer, M. J., Matzinger, M., Müller, F., Mechtler, K. & Dorfer, V. MS Annika 2.0 Identifies Cross-Linked Peptides in MS2–MS3-Based Workflows at High Sensitivity and Specificity. *J. Proteome Res.* (2023) doi:10.1021/acs.jproteome.3c00325.
43. Birklbauer, M. J. *et al.* Proteome-wide non-cleavable crosslink identification with MS Annika 3.0 reveals the structure of the C. elegans Box C/D complex. *bioRxiv* 2024.09.03.610962 (2024) doi:10.1101/2024.09.03.610962.
44. Nelli, F. *Pandas in 7 Days: Utilize Python to Manipulate Data, Conduct Scientific Computing, Time Series Analysis, and Exploratory Data Analysis (English Edition)*. (BPB Publications, 2022).
45. Harris, C. R. *et al.* Array programming with NumPy. *Nature* **585**, 357–362 (2020).
46. Hunter, J. D. Matplotlib: A 2D Graphics Environment. *Comput. Sci. Eng.* **9**, 90–95 (2007).
47. Waskom, M. seaborn: statistical data visualization. *J. Open Source Softw.* **6**, 3021 (2021).
48. Garreta, R. & Moncecchi, G. *Learning Scikit-Learn: Machine Learning in Python*. (Packt Pub Limited, 2013).
49. Virtanen, P. *et al.* SciPy 1.0: fundamental algorithms for scientific computing in Python. *Nat. Methods* **17**, 261–272 (2020).
50. Perez-Riverol, Y. *et al.* The PRIDE database at 20 years: 2025 update. *Nucleic Acids Res* (2024) doi:10.1093/nar/gkae1011.
51. Perez-Riverol, Y. *et al.* The PRIDE database resources in 2022: a hub for mass spectrometry-based proteomics evidences. *Nucleic Acids Res* **50**, D543–D552 (2022).

Acknowledgements

This work was supported by the infrastructure funding 4*th* call 2022/01 (AT-SCP) of the Austrian Research Promotion Agency (FFG). This work was further funded by the ESPRIT program project number ESP 566 (Grant-DOI 10.55776/ESP566) and the F 8801-B Meiosis project (Grant-DOI 10.55776/F88) of the Austrian Science Fund (FWF). All LC-MS/MS analyses in Vienna were performed on the Vienna BioCenter Core Facilities instrument pool. We thank the MS core facility headed by Elisabeth Roitinger for support and help with setting up the Orbitrap Eclipse mass spectrometer. Furthermore, we thank Julia Bubis and Rupert Mayer for proofreading and suggestions.

This research was funded in whole, or in part, by the Austrian Science Fund (FWF). For open access purposes, the author has applied a CC BY public copyright license to any author-accepted manuscript version arising from this submission.

Competing interest statement

The authors declare no competing interest.

Ethics approval and consent to participate

Not applicable.